

# Optical signatures of Mott-superfluid transition in nitrogen-vacancy centers coupled to photonic crystal cavities

Jia-Bin You,<sup>1,2</sup> W. L. Yang,<sup>1,\*</sup> G. Chen,<sup>3</sup> Z. Y. Xu,<sup>4</sup> Lin Wu,<sup>2</sup> Ching Eng Png,<sup>2</sup> and M. Feng<sup>1,†</sup>

<sup>1</sup>State Key Laboratory of Magnetic Resonance and Atomic and Molecular Physics, Wuhan Institute of Physics and Mathematics, Chinese Academy of Sciences, Wuhan 430071, China

<sup>2</sup>Department of Electronics and Photonics, Institute of High Performance Computing, 1 Fusionopolis Way, 16-16 Connextis, Singapore 138632, Singapore

<sup>3</sup>State Key Laboratory of Quantum Optics and Quantum Optics Devices, Institute of Laser Spectroscopy, Shanxi University, Taiyuan 030006, China

<sup>4</sup>College of Physics, Optoelectronics and Energy, Soochow University, Suzhou 215006, China

We study the phenomenon of controllable localization-delocalization transition in a quantum many-body system composed of nitrogen-vacancy centers coupled to photonic crystal cavities, through tuning the different detunings and the relative amplitudes of two optical fields that drive two nondegenerate transitions of the  $\Lambda$ -type configuration. We not only characterize how dissipation affects the phase boundary using the mean-field quantum master equation, but also provide the possibility of observing this photonic quantum phase transition (QPT) by employing several experimentally observable quantities, such as mean intracavity photon number, density correlation function and emitted spectrum, exhibiting distinct optical signatures in different quantum phases. Such a spin-cavity system opens new perspectives in quantum simulation of condensed-matter and many-body physics in a well-controllable way.

*Introduction.*— Using quantum hybrid systems to simulate condensed-matter and many-body physics is an exciting frontier of physics [1–8]. Among the promising platforms, the scalable coupled microcavities (superconducting resonators) array doped with quantum emitters (superconducting qubit) [9–19] has received much attention. Especially, the integrated photonic networks based on cavity-emitter coupled systems, such as nitrogen vacancy centers (NVC) or cold atom interfaced with photonic crystal cavity (PCC) provide a powerful platform for studying the strongly-correlated states of light and nonequilibrium quantum phase transition (QPT) [20–25]. Despite this remarkable success, realizing controllable light-matter interaction between electromagnetic quanta and discrete levels of quantum system in highly scalable devices is a serious challenge. Additionally, considerably less attention has been paid to the detection of nonequilibrium QPT phenomena in these hybrid systems, therefore new important questions arise related to whether it is possible to more visually observe and detect the optical signature and critical characteristic of QPT using experimentally observable quantities.

To this end, the present work focus on a hybrid NVC-PCC system, where each site composed of a nanocavity and a NVC. Through tuning the polariton states that are hybridizations of photon and NVC by implementing a dipole-allowed  $\Lambda$ -type transition configuration established by localized tunable cavity mode and external laser driving, a well-controllable QPT of light could be realized via full photonic process. In this artificially engineered hybrid devices, NVC exhibits excellent optical coherence

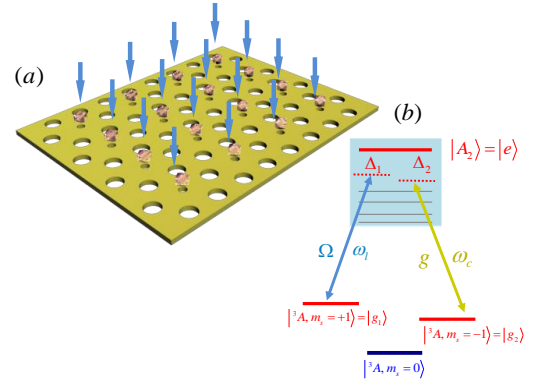


FIG. 1. (a) The system under consideration consists of a 2D planar PCC coupled to NVC, where each nanocavity embeds a single NVC, and the parallel arrows above the NVC denote the classical laser pulses. (b) The level structure of NVC, where the nanocavity mode and an external control laser field drive the transitions from the two NVC’s ground states  $|g_1\rangle$  and  $|g_2\rangle$  to the excited state  $|e\rangle$ .

properties at ambient conditions and efficient optical control and readout [26–34]. Additionally, a PCC is a periodic dielectric structure that seeds a localized, tunable cavity mode around the NVC and controls the propagation of light [21]. When many NVCs are trapped, these dynamically induced cavities mediate coherent interactions between NVCs [35, 36]. Our proposal is inspired by series of experimental demonstrations on strong coupling or quantum properties of photons in nanophotonic systems with individual solid-state emitters [22–25], ion [37] or cold atom [21, 38].

The goal of the present work is twofold. On the one hand, based the composite NVC-PCC system, we attempt to demonstrate a controllable localization-

\* ywl@wipm.ac.cn

† mangfeng@wipm.ac.cn

delocalization transition of light by virtue of Raman transition through adjusting the key parameters for quantum control, which can be dynamically tuned using available structures of tunable cavity mode and adjusting external controlling laser fields. Besides exhibiting a complete picture for the driven-dissipation QPT using the Mean-field quantum Master equation (MME), the high degree of controllability also opens up new possibilities for studying strongly-correlated photon physics in a well-controlled way. One the other hand, we address the issue of detecting optical signatures of QPT by calculate the behavior of mean photon number, photon fluctuation, equal-time correlation function, and emitted spectrum in complete parameter space. We find that these observable quantities exhibiting distinct optical signatures in different quantum phases and could be a good indicator of dissipative QPT.

*The model and Hamiltonian.*- As illustrated in Fig. 1(a), the system under consideration consists of a PCC where each NVC is embedded in the localized nanocavity with frequency and nonlocal hopping rate tunable by changing geometrical parameters of the defects [39–43]. The ground state sublevels are  $|g_1\rangle = |^3A, m_s = +1\rangle$  and  $|g_2\rangle = |^3A, m_s = -1\rangle$  with radiation of  $\sigma^-$  and  $\sigma^+$  circular polarizations, respectively, whereas the excited level is  $|e\rangle = |A_2\rangle$  within the spin-orbit excited state manifold [44, 45]. The  $|g_1\rangle$  spin state of NVC is linked to  $|A_2\rangle$  by an off-resonant laser pulse with detuning  $\Delta_1$ , strength  $\Omega$  and frequency  $\omega_l$ , while the transition  $|g_2\rangle \leftrightarrow |A_2\rangle$  is driven by the nanocavity mode with detuning  $\Delta_2$ , strength  $g$  and frequency  $\omega_c$  [46, 47]. This particularly useful  $\Lambda$ -type transition was recently employed for spin-photon entanglement production [48], high-fidelity transfer [33], and holonomic quantum gate [34] in experiments.

Setting the energy of level  $|g_1\rangle$  to zero, the effective Hamiltonian at the  $i$ -th site can be written under a rotating wave approximation in units of  $\hbar = 1$  as  $H_i = \omega_e|e\rangle\langle e| + \omega_2|g_2\rangle\langle g_2| + \omega_c a^\dagger a + \Omega[|g_1\rangle\langle e|e^{i\omega_l t} + |e\rangle\langle g_1|e^{-i\omega_l t}] + g[|g_2\rangle\langle e|a^\dagger + a|e\rangle\langle g_2|]$ , where  $\omega_e = \omega_l + \Delta_1$ , and  $\omega_2 = \omega_l - \omega_c + \Delta_1 - \Delta_2$  with  $a^\dagger(a)$  the creation (annihilation) operator of photon. In the interaction picture the Hamiltonian  $H_i$  can be reduced as

$$H_i^0 = \sum_{i=1,3} \Delta_i \sigma_i^+ \sigma_i^- + (\Omega \sigma_1^+ + g a \sigma_2^+ + h.c.), \quad (1)$$

where  $\Delta_3 = \Delta_1 - \Delta_2$ , and the lowering and raising operators are defined as  $\sigma_1^+ = |e\rangle\langle g_1|$ ,  $\sigma_2^+ = |e\rangle\langle g_2|$  and  $\sigma_3^+ = |g_2\rangle\langle g_1|$ . Note that the total number of excitations  $N_i = a_i^\dagger a_i + \sigma_{i,1}^+ \sigma_{i,1}^- + \sigma_{i,3}^+ \sigma_{i,3}^-$  is the conserved quantity of the system. Adding the on-site chemical potential and the adjacent-site photon hopping, the full Hamiltonian for the 2D square lattice is given by

$$H = \sum_i H_i^0 - \sum_{\langle i,j \rangle} k_{ij} a_i^\dagger a_j - \sum_i \mu_i N_i. \quad (2)$$

The second term in Eq. (2) describes the the nonlocal hopping of photons between nearest-neighbor nanocav-

ities with the hopping rate  $k_{i,j}$ . The third term in Eq.(2) describes the on-site chemical potential with the value  $\mu_i$  at the  $i$ -th site, which is conceptually different from the chemical potential in electronic system. For convenience to determine the phase diagram, we used the grand canonical approach considering a situation in which particle exchange with the surroundings is permitted [49], and we assume zero disorder with  $\mu_i = \mu$  and  $k_{ij} = k$  for all sites.

*Dissipative QPT.*- Using the mean-field theory [50, 51] we decouple the hopping term as  $a_i^\dagger a_j = \langle a_i^\dagger \rangle a_j + a_i^\dagger \langle a_j \rangle - \langle a_i^\dagger \rangle \langle a_j \rangle$  and make a sum over single sites, the mean-field Hamiltonian can be written as

$$H^m = \sum_i [H_i^0 - zk(a_i \psi_a^* + a_i^\dagger \psi_a) + zk|\psi_a|^2 - \mu_i N_i], \quad (3)$$

where the periodic boundary condition is applied, and  $z = 4$  is the coordination number of the lattice.

We choose the superfluid (SF) phase order parameter  $\psi_a = \langle a_i \rangle$  (set to be real) to differentiate the different phases. Minimizing the ground state energy of the Hamiltonian  $H^m$  (Eq.(3)) with respect to  $\psi_a$  for different values of  $\mu$  and  $k$ , we obtain the mean field phase diagram/boundary in the  $(\mu, k)$  plane for different tunable parameters, as shown in Fig. 2. When the on-site large repulsion resulting from laser-assisted spin-cavity coupling dominates ( $k \ll g_{eff} = (\Delta_1 + \Delta_2)g\Omega/(2\Delta_1\Delta_2)$ ), the system is in the Mott insulator (MI) phase with  $\psi_a = 0$ , which obeys the  $U(1)$  gauge transformation. In the incompressible MI phase characterized by a fixed number of excitations at per site with no variance, the photon fluctuations in each nanocavity are suppressed due to the strong nonlinearity and anharmonicity in the spectrum originating from the photon blockade effect [52], and the on-site repulsive interaction between the local photons freezes out hopping and localizes polaritons at individual lattice sites. By contrast, when the hopping process with  $k \gg g_{eff}$  dominates the dynamics, strong hopping favours delocalization and condensation of the particles, therefore the system prefers a  $U(1)$ -symmetry broken SF phase with  $\psi_a \neq 0$ . In the compressible SF phase with non-integer polariton number and large fluctuation, the lowest-energy state of the system is a condensate of delocalized polariton, and the stable ground state at each site corresponds to a coherent state of excitations [x]. Therefore, The physical picture behind is that the MI-SF phase transition results from the interplay between on-site repulsive interaction and polariton delocalization.

Note that  $H^m$  is invariant under an  $U(1)$  gauge transform:  $\psi_a \rightarrow \psi_a e^{i\phi}$ ,  $a \rightarrow a e^{i\phi}$ ,  $\sigma_1^+ \rightarrow \sigma_1^+ e^{-i\phi}$ , implying that all odd-order terms in the expansion of  $E_g(\psi_a)$  vanish [53]. Therefore, the ground-state energy has an expression  $E_g(\psi_a) = E_g^0 + (zk + r)|\psi_a|^2 + u|\psi_a|^4 + O(|\psi_a|SF^6)$ , where  $E_g^0$  is ground state energy of the Hamiltonian  $\tilde{H} = \sum_i (H_i^0 - \mu N_i)$ . From Landau phase transition theory [x] and second-order perturbation theory, the MI-SF transition occurs when  $zk + r = 0$ ,

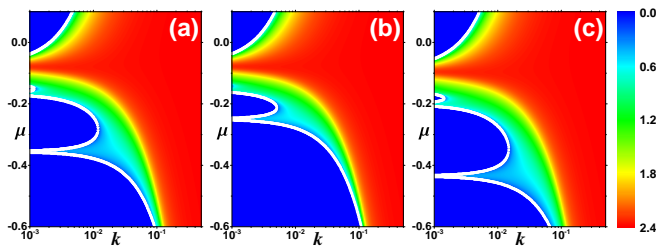


FIG. 2. Phase diagrams in the  $\mu \sim k$  plane for different parameters. The common parameters are  $g = 1$  (used in all the Figures). (a)  $\Omega = 5$ ,  $\Delta_1 = 4$ ,  $\Delta_2 = -2.5$ ; (b)  $\Omega = 5$ ,  $\Delta_1 = 4.3$ ,  $\Delta_2 = -2.5$ ; (c)  $\Omega = 4.2$ ,  $\Delta_1 = 3.3$ ,  $\Delta_2 = -2.1$ . The color scale shows the magnitude of the order parameter  $\psi_a$ . The white contour is the SF-MI phase boundary.

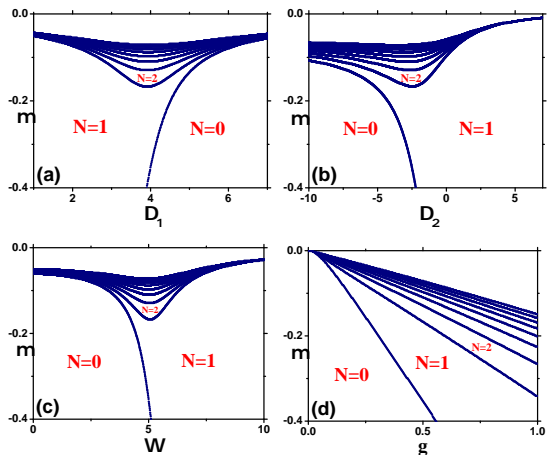


FIG. 3. Boundaries between MI lobes in the limit of low tunnelling ( $k \approx 0$ ) as a function of detunings and couplings. The parameters in each figure are the same as Fig. (2a).

then we obtain the phase boundary line calculated from  $r = (zk)^2 \sum_{m \neq n} | \langle m^0 | (a + a^\dagger) | n^0 \rangle |^2 / (E_n^0 - E_m^0)$ , which is plotted by the white contour in Fig. 2, where  $|n^0\rangle$  ( $E_n^0$ ) is the eigenstate (eigenenergy) of Hamiltonian  $\tilde{H}$ .

Fig. 2 tells us that phase boundary and size of the MI lobes primarily depend on the ratio of on-site repulsion rate to hopping rate, and it could also be shifted and changed by adjusting the controllable parameters  $\{\Omega, \Delta_1, \Delta_2\}$ . We visualize the corresponding boundary lines between MI lobes labelled with different polariton number  $\langle N \rangle$  for the ground state of Hamiltonian  $\tilde{H}$  in Fig. 3. The Fig. 3(a,b) show the boundary lines as a function of detunings  $\Delta_1$  and  $\Delta_2$ , and there exist an optimal detuning value which induces the MI lobes with the most obvious separation. Any deviation from this optimal detuning  $\Delta_1$  ( $\Delta_2$ ) will lead to symmetric (asymmetric) convergence of the MI lobes whose polariton number greater than one. From Fig. 3(c,d), we find that the phenomena of QPT disappear once on-site repulsive interaction turns off through setting  $\Omega = 0$  or  $g = 0$ .

Taking account of dissipation effects of polariton

states, which resulting from the decays of both cavity fields and NVCs, we simulate the non-equilibrium dynamics by integrating the MME with the following form

$$\dot{\rho} = -i[H^m, \rho] + \frac{\kappa}{2} D[a]\rho + \sum_{i=1,2} \frac{\Gamma_i}{2} D[\Gamma_i]\rho, \quad (4)$$

where  $D[A]\rho = 2A\rho A^\dagger - A^\dagger A\rho - \rho A^\dagger A$ ,  $\kappa$  is the nanocavity decay rate, and  $\Gamma_1$  ( $\Gamma_2$ ) are the spontaneous decay rates from excited state  $|e\rangle$  to ground states  $|g_1\rangle$  ( $|g_2\rangle$ ). The dissipative phase diagram is shown in Fig. 4. It is found that the MI-lobe structure gradually disappear and the area of MI phase expands as the dissipation strength increases, i.e., new MI phase forms in the SF phase region existing in the dissipationless case. The values of  $\psi_a$  also decrease when the dissipation effects are considered. In the MI phase, the dissipation has a greater influence on the region with higher  $\langle N \rangle$ . For a certain  $\mu$ , the value of  $\psi_a$  near the phase boundary is bigger than that away from the phase boundary. In contrast, the dissipation effect slightly increase  $\psi_a$  in the SF phase. Surprisingly, we observe that there exists an oscillatory region in the SF phase region. This is due to the emergence of multi-steady state resulting from the mean-field approximation [16, 54], and this multi-stability will disappear once the spatial quantum correlations are considered.

*Detection of the QPT.*- We pay particular attention to using the physical observable quantities to detect the QPT in the present system. Note that the global signatures of the transition, such as the order parameter and compressibility, are revealed in the photon number. Therefore we study the critical behavior of mean intracavity photon number  $\langle n_a \rangle$ , photon fluctuation  $\langle (\Delta n_a)^2 \rangle$  and 2nd-order equal-time correlation function  $g^{(2)}(0)$ , which allows one to identify the optical signatures of the QPT, as shown in Fig. 5, where we plot  $\langle n_a \rangle$ ,  $\langle (\Delta n_a)^2 \rangle$ , and  $g^{(2)}(0)$  as a function of hopping rate  $k$  for different  $\mu$ , computed from steady state solutions of the MME. In Fig. 5(a), the photon number  $\langle n_a \rangle$  is integer (non-integer) in the MI (SF) phase in the dissipationless case. In contrast,  $\langle n_a \rangle$  always decays to zero in MI phase, and quickly converges in SF phase when  $k$  increases in the dissipation case (Fig. 5(d)). The Fig. 5(b,e) reveal that quantum fluctuations arising from Heisenberg's uncertainty relation drive the transition from MI phase to SF phase because the value of  $\langle (\Delta n_a)^2 \rangle$  is zero (nonzero) in MI (SF) phase. In the dissipationless case (Fig. 5(b)), the maximal fluctuation occurs near the phase boundary and undergoes a discontinuous change with a cusp-like character, then converges to a finite value at large  $k$ . In the dissipation case (Fig. 5(e)), the fluctuation abruptly arises at the phase boundary and gradually converges at a larger value compared with the dissipationless case.

The density correlation function defined by  $g^{(2)}(0) = \langle a^\dagger a^\dagger a a \rangle / \langle a^\dagger a \rangle^2$  also exhibits distinct behaviors in different phases. In the dissipationless case (Fig. 5(c)), we find that  $g^{(2)}(0) < 1$  in MI phase indicates photon

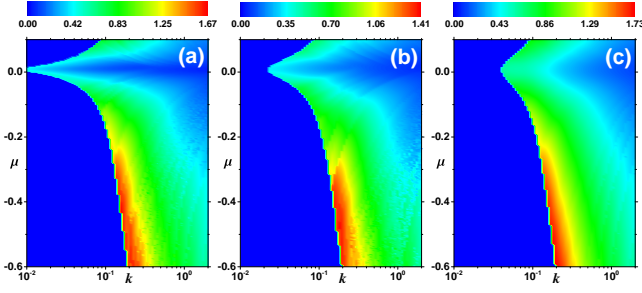


FIG. 4. Dissipative quantum phase diagrams in the  $\mu \sim k$  plane for different parameters.  $\Omega = 5$ ,  $\Delta_1 = 4$ ,  $\Delta_2 = -2.5$ ; (a)  $\Gamma_1 = \Gamma_2 = 0.01$ ,  $\kappa = 0.01$ ; (b)  $\Gamma_1 = \Gamma_2 = 0.05$ ,  $\kappa = 0.01$ ; (c)  $\Gamma_1 = \Gamma_2 = 0.05$ ,  $\kappa = 0.05$ .

antibunching with sub-Poissonian statistics and photon blockade, and  $g^{(2)}(0)$  gradually converges around 1 in SF phase with the growth of  $k$ . The dissipation case (Fig. 5(f)) exhibits a sudden transition of  $g^{(2)}(0)$  from strong photon antibunching ( $g^{(2)}(0) \ll 1$ ) to photon bunching ( $g^{(2)}(0) > 1$ ) with super-Poissonian statistics if we continuously increase  $k$ . Note that  $g^{(2)}(0) = 1 + [\langle(\Delta n)^2\rangle - \langle n \rangle] / \langle n \rangle^2 < 1$  due to zero variance ( $\Delta n = 0$ ) and constant photon number in MI phase, whereas  $g^{(2)}(0) = 1$  in SF phase because it could be represented by a coherent state  $|\alpha\rangle$  with non-integer polariton number and large fluctuation [55]. In the experiments one can infer the cavity field quadrature amplitudes, intracavity photon number, and photon correlations by continuously monitoring the output of PCC through available photon detectors [56, 57]. Additionally, the measurements of  $g^{(2)}(0)$  could be accessed by a modified heterodyne/homodyne or a Hanbury-Brown-Twiss setup [58], and a recent experiment made a direct measurement of  $g^{(2)}(0)$  on NVC by the characterization of fluorescent objects [59].

The normalized emitted spectrum (NES) of system is another excellent optical signature to detect the different phases. Next we turn to study the two-time correlation function, whose spectral counterpart corresponds to a concrete readily measurable quantity. Specifically, we show how to detect the MI-SF phase transition for this dissipative-driven system, through distinguishing NES in different phases. It is convenient to calculate the NES by combining Wiener-Khinchine theorem [60, 61] with MME, and it can be written as

$$S_\alpha(\omega) = \frac{1}{\pi n_\alpha^{SS}} \lim_{t \rightarrow \infty} \text{Re} \int_0^\infty G_\alpha^{(1)}(t, \tau) e^{i\omega\tau} d\tau, \quad (5)$$

where the first-order time autocorrelator is  $G_\alpha^{(1)}(t, \tau) = \langle \alpha^\dagger(t)\alpha(t+\tau) \rangle - |\langle \alpha(t) \rangle|^2$ , and  $n_\alpha^{SS}$  is the steady-state photon number with  $\alpha = a, \sigma_1^-, \sigma_2^-$  [62].

Note that in the dissipation case the steady photon number  $n_\alpha^{SS} = 0$  when the system is in MI phase (Fig. 5(d)), there is nothing could be observed in the NES. In contrast, the hopping term under mean-field approximation in Eq. (3) is similar to a coherent pumping

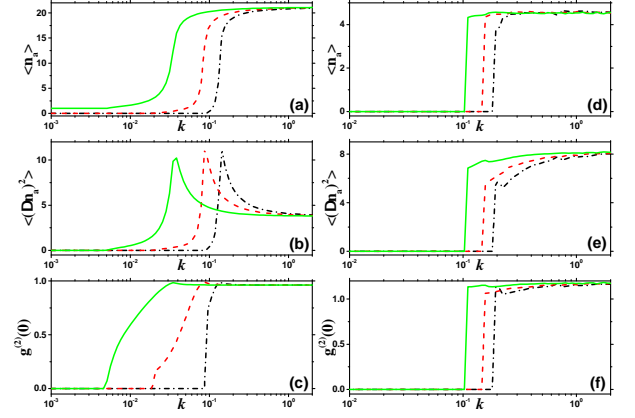


FIG. 5. Mean intracavity photon number  $\langle n_a \rangle$  (top), photon fluctuation  $\langle (\Delta n_a)^2 \rangle$  (middle) and intensity correlation function  $g^{(2)}(0)$  (bottom) as a function of hopping rate  $k$  for  $\mu = -0.6$  (black line),  $-0.4$  (red line),  $-0.2$  (green line). (a), (b), (c) are for dissipationless case with the same parameters in Fig. (2a). (d), (e), (f) are for dissipation case with the same parameters in Fig. (4a).

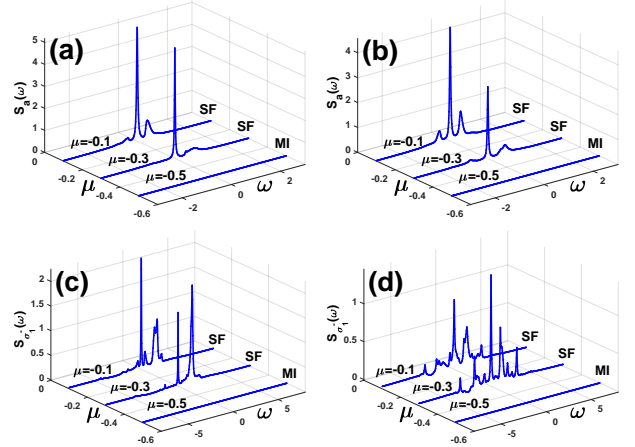


FIG. 6. NES of nanocavity in the different phases. The parameters are (a,c)  $\Delta_1 = 4$ ,  $\Delta_2 = -2.5$ ,  $\Omega = 0$ ,  $\eta = 0.05$ ,  $k = 0.13$ ,  $\mu = -0.1, -0.3, -0.5$ ; (b,d)  $\Delta_1 = 4$ ,  $\Delta_2 = -2.5$ ,  $\Omega = 5$ ,  $\eta = 0.05$ ,  $k = 0.13$ ,  $\mu = -0.1, -0.3, -0.5$ .

when  $\psi_a$  is nonzero in SF phase. Fig. 6 show the NES of nanocavity in different phases, where the lineshape of NES of nanocavity  $S_\alpha(\omega)$  is the standard "Mollow triplet" ("Straight line") in SF (MI) phase (Fig. 6(a,b)), and the intensity and location of the sideband peaks can be changed by the chemical potential. Therefore, the NES of nanocavity could also be a good indicator of dissipative QPT.

*Summary.*- In conclusion, we propose a composite NVC-PCC system for engineering a photonic QPT in a well-controllable way, where the effective on-site repulsion can be tuned by changing the laser frequency and intensity, while the cavity frequency and hopping strength

could be adjusted by the geometrical parameters of the defects. The NVCs remains individually addressable, full control at the single-particle level, and site-resolved measurement. The physical behind MI-SF phase transition is that quantum fluctuations arising from Heisenberg's uncertainty relation drive the transition. We also focus on using several experimentally observable quantities exhibiting distinct optical signatures in different quantum phases to detect the localization-delocalization transition. Our work opens new perspectives in quantum

simulation of condensed-matter and many-body physics using such a 2D spin-cavity system.

This work was supported by the National Key Research and Development Program of China under Grant No. 2017YFA0304503 and by the National Natural Science Foundation of China under Grant No. 11574353. The IHPC A\*STAR Team would like to acknowledge the National Research Foundation Singapore (Grant No. NRF2017NRF-NSFC002-015, NRF2016-NRF-ANR002, NRF-CRP 14-2014-04) and A\*STAR SERC (Grant No. A1685b0005).

- 
- [1] A. D. Greentree, C. Tahan, J. H. Cole, and L. C. L. Hollenberg, *Nat. Phys.* **2**, 849 (2006).
- [2] M. J. Hartmann, F. G. S. L. Brandao, and M. B. Plenio, *Nat. Phys.* **2**, 856 (2006).
- [3] D. G. Angelakis, M. F. Santos, and S. Bose, *Phys. Rev. A* **76**, 031805 (2007).
- [4] C. Noh and D. G. Angelakis, *Reports on Progress in Physics* **80**, 016401 (2017).
- [5] M. Schiró, C. Joshi, M. Bordyuh, R. Fazio, J. Keeling, and H. E. Türeci, *Phys. Rev. Lett.* **116**, 143603 (2016).
- [6] B. Yang, Y.-Y. Chen, Y.-G. Zheng, H. Sun, H.-N. Dai, X.-W. Guan, Z.-S. Yuan, and J.-W. Pan, *Phys. Rev. Lett.* **119**, 165701 (2017).
- [7] M.-J. Hwang, P. Rabl, and M. B. Plenio, *Phys. Rev. A* **97**, 013825 (2018).
- [8] L.-L. Zheng, K.-M. Li, X.-Y. Lü, and Y. Wu, *Phys. Rev. A* **96**, 053809 (2017).
- [9] G. Lepert, M. Trupke, M. J. Hartmann, M. B. Plenio, and E. A. Hinds, *New Journal of Physics* **13**, 113002 (2011).
- [10] W. L. Yang, Z.-q. Yin, Z. X. Chen, S.-P. Kou, M. Feng, and C. H. Oh, *Phys. Rev. A* **86**, 012307 (2012).
- [11] J. Raftery, D. Sadri, S. Schmidt, H. E. Türeci, and A. A. Houck, *Phys. Rev. X* **4**, 031043 (2014).
- [12] A. Houck, H. E. Türeci, and J. Koch, *Nat. Phys.* **8**, 292 (2012).
- [13] A. Wallraff, D. I. Schuster, A. Blais, L. Frunzio, R.-S. Huang, J. Majer, S. Kumar, S. M. Girvin, and R. J. Schoelkopf, *Nature (London)* **431**, 162 (2004).
- [14] I. Chiorescu, P. Bertet, K. Semba, Y. Nakamura, C. J. P. M. Harmans, and J. E. Mooij, *Nature (London)* **431**, 159 (2004).
- [15] I. M. Georgescu, S. Ashhab, and F. Nori, *Rev. Mod. Phys.* **86**, 153 (2014).
- [16] J. Jin, D. Rossini, R. Fazio, M. Leib, and M. J. Hartmann, *Phys. Rev. Lett.* **110**, 163605 (2013).
- [17] T. Aoki, B. Dayan, E. Wilcut, W. P. Bowen, A. S. Parkins, T. J. Kippenberg, K. J. Vahala, and H. J. Kimble, *Nature (London)* **443**, 671 (2006).
- [18] K. Hennessy, A. Badolato, M. Winger, D. Gerace, M. Atatüre, S. Gulde, S. Fält, E. L. Hu, and A. Imamoglu, *Nature (London)* **445**, 896 (2007).
- [19] M. Trupke, J. Goldwin, B. Darquié, G. Dutier, S. Eriksson, J. Ashmore, and E. A. Hinds, *Phys. Rev. Lett.* **99**, 063601 (2007).
- [20] W. B. Gao, A. Imamoglu, H. Bernien, and R. Hanson, *Nat. Photon.* **9**, 363 (2015).
- [21] J. S. Douglas, H. Habibian, C.-L. Hung, A. V. Gorshkov, H. J. Kimble, and C. D. E., *Nat. Photon.* **9**, 326 (2015).
- [22] O. Benson, *Nature (London)* **480**, 193 (2011).
- [23] A. Faraon, P. E. Barclay, C. Santori, K.-M. C. Fu, and R. G. Beausoleil, *Nat. Photon.* **5**, 301 (2011).
- [24] G. Khitrova, H. M. Gibbs, M. Kira, S. W. Koch, and A. Scherer, *Nat. Phys.* **2**, 81 (2006).
- [25] G. Calusine, A. Politi, and D. D. Awschalom, *Appl. Phys. Lett.* **105**, 011123 (2014).
- [26] P. C. Maurer, G. Kucsko, C. Latta, L. Jiang, N. Y. Yao, S. D. Bennett, F. Pastawski, D. Hunger, N. Chisholm, M. Markham, D. J. Twitchen, J. I. Cirac, and M. D. Lukin, *Science* **336**, 1283 (2012).
- [27] T. van der Sar, Z. H. Wang, M. S. Blok, H. Bernien, T. H. Taminiau, D. M. Toyli, D. A. Lidar, D. D. Awschalom, R. Hanson, and V. V. Dobrovitski, *Nature (London)* **484**, 82 (2012).
- [28] L. Robledo, L. Childress, H. Bernien, B. Hensen, P. F. A. Alkemade, and R. Hanson, *Nature (London)* **477**, 574 (2011).
- [29] W. Ma, L. Zhou, Q. Zhang, M. Li, C. Cheng, J. Geng, X. Rong, F. Shi, J. Gong, and J. Du, *Phys. Rev. Lett.* **120**, 120501 (2018).
- [30] W. Ma, B. Chen, Y. Liu, M. Wang, X. Ye, F. Kong, F. Shi, S.-M. Fei, and J. Du, *Phys. Rev. Lett.* **118**, 180402 (2017).
- [31] S. Putz, A. Angerer, D. O. Krimer, R. Glattauer, W. J. Munro, S. Rotter, J. Schmiedmayer, and J. Majer, *Nat. Photon.* **11**, 36 (2017).
- [32] S. E. Lillie, D. A. Broadway, J. D. A. Wood, D. A. Simpson, A. Stacey, J.-P. Tetienne, and L. C. L. Hollenberg, *Phys. Rev. Lett.* **118**, 167204 (2017).
- [33] S. Yang, Y. Wang, D. D. Bhaktavatsala Rao, T. H. Tran, A. S. Momenzadeh, M. Markham, D. J. Twitchen, P. Wang, W. Yang, R. Stöhr, P. Neumann, H. Kosaka, and J. Wrachtrup, *Nat. Photon.* **10**, 507 (2016).
- [34] Y. Sekiguchi, N. Niikura, R. Kuroiwa, H. Kano, and H. Kosaka, *Nat. Photon.* **11**, 309 (2017).
- [35] G. Kurizki, *Phys. Rev. A* **42**, 2915 (1990).
- [36] S. John and J. Wang, *Phys. Rev. B* **43**, 12772 (1991).
- [37] T. Utikal, E. Eichhammer, L. Petersen, A. Renn, S. Götzinger, and V. Sandoghdar, *Nat. Commun.* **5**, 3627 (2014).
- [38] J. D. Thompson, T. G. Tiecke, N. P. de Leon, J. Feist, A. V. Akimov, M. Gullans, A. S. Zibrov, V. Vuletić, and M. D. Lukin, *Science* **340**, 1202 (2013).
- [39] X.-y. Guo and S.-c. Lü, *Phys. Rev. A* **80**, 043826 (2009).
- [40] K. Zhang and Z.-Y. Li, *Phys. Rev. A* **81**, 033843 (2010).
- [41] X. Guo and Z. Ren, *Phys. Rev. A* **83**, 013809 (2011).

- [42] M. Knap, E. Arrigoni, W. von der Linden, and J. H. Cole, *Phys. Rev. A* **83**, 023821 (2011).
- [43] H.-T. Tan, W.-M. Zhang, and G.-x. Li, *Phys. Rev. A* **83**, 062310 (2011).
- [44] J. R. Maze, A. Gali, E. Togan, Y. Chu, A. Trifonov, E. Kaxiras, and M. D. Lukin, *New Journal of Physics* **13**, 025025 (2011).
- [45] B. B. Zhou, P. C. Jerger, V. O. Shkolnikov, F. J. Heremans, G. Burkard, and D. D. Awschalom, *Phys. Rev. Lett.* **119**, 140503 (2017).
- [46] C. Santori, P. Tamarat, P. Neumann, J. Wrachtrup, D. Fattal, R. G. Beausoleil, J. Rabeau, P. Olivero, A. D. Greentree, S. Praver, F. Jelezko, and P. Hemmer, *Phys. Rev. Lett.* **97**, 247401 (2006).
- [47] P. Tamarat, N. B. Manson, J. P. Harrison, R. L. McMurry, A. Nizovtsev, C. Santori, R. G. Beausoleil, P. Neumann, T. Gaebel, F. Jelezko, P. Hemmer, and J. Wrachtrup, *New Journal of Physics* **10**, 045004 (2008).
- [48] E. Togan, Y. Chu, A. S. Trifonov, L. Jiang, J. Maze, L. Childress, M. V. G. Dutt, A. S. Sorensen, P. R. Hemmer, A. S. Zibrov, and M. D. Lukin, *Nature (London)* **466**, 730 (2010).
- [49] M. Hartmann, F. Brandao, and M. Plenio, *Laser & Photonics Reviews* **2**, 527.
- [50] D. van Oosten, P. van der Straten, and H. T. C. Stoof, *Phys. Rev. A* **63**, 053601 (2001).
- [51] D. van Oosten, P. van der Straten, and H. T. C. Stoof, *Phys. Rev. A* **67**, 033606 (2003).
- [52] K. M. Birnbaum, A. Boca, R. Miller, A. D. Boozer, T. E. Northup, and H. J. Kimble, *Nature (London)* **436**, 87 (2005).
- [53] J. Koch and K. Le Hur, *Phys. Rev. A* **80**, 023811 (2009).
- [54] J. J. Mendoza-Arenas, S. R. Clark, S. Felicetti, G. Romero, E. Solano, D. G. Angelakis, and D. Jaksch, *Phys. Rev. A* **93**, 023821 (2016).
- [55] R. J. Glauber, *Phys. Rev.* **130**, 2529 (1963).
- [56] A. Tomadin, V. Giovannetti, R. Fazio, D. Gerace, I. Carusotto, H. E. Türeci, and A. Imamoglu, *Phys. Rev. A* **81**, 061801 (2010).
- [57] M. França Santos, L. G. Lutterbach, S. M. Dutra, N. Zangury, and L. Davidovich, *Phys. Rev. A* **63**, 033813 (2001).
- [58] D. Walls and G. Milburn, *Quantum Optics* (Springer-Verlag, New York, 1994).
- [59] E. Moreva, P. Traina, J. Forneris, I. P. Degiovanni, S. Ditalia Tchernij, F. Picollo, G. Brida, P. Olivero, and M. Genovese, *Phys. Rev. B* **96**, 195209 (2017).
- [60] F. P. Laussy, E. del Valle, and C. Tejedor, *Phys. Rev. B* **79**, 235325 (2009).
- [61] M. O. Scully and M. S. Zubairy, *Quantum Optics* (Cambridge University Press, 1997).
- [62] A. Nummenkamp, K. Børkje, and S. M. Girvin, *Phys. Rev. Lett.* **107**, 063602 (2011).